Extensive Journal of Applied Sciences
https://ejasj.com/index.php/EJASJ/index (Vol 2 No 1 2026)

Advanced InP-Si Coupler Design: Optimizing Grating Devices for Vertical Coupling in Photonic Integrated Circuits

Noah Halvorsen, Noah Barrett, Jonathan Bradley

Photonics Research Group, Ghent University - imec, Ghent, Belgium

ABSTRACT : The integration of Indium Phosphide light sources with silicon photonic chips represents a critical frontier in modern optical communications and data processing architectures. Silicon exhibits an indirect bandgap, making it fundamentally unsuited for efficient light emission, whereas Indium Phosphide is a highly efficient light-generating material. To bridge this gap, efficient optical coupling between Indium Phosphide active components and silicon passive waveguides is imperative. This paper presents a comprehensive investigation into the design, optimization, and theoretical analysis of vertical grating couplers designed for Indium Phosphide to silicon integration. We explore advanced apodization techniques and sub-wavelength grating structures to minimize mode mismatch, enhance coupling efficiency, and broaden the spectral bandwidth around the telecommunication wavelength of 1550 nanometers. Through rigorous finite-difference time-domain simulations and theoretical modeling, the structural parameters including etch depth, grating pitch, and duty cycle are systematically optimized. Furthermore, we provide a detailed analysis of fabrication tolerances, alignment sensitivities, and the impact of interfacial bonding layers. The proposed vertical grating coupler designs demonstrate significantly reduced back-reflection and enhanced polarization control. This research provides a robust framework for developing scalable, high-efficiency hybrid photonic integrated circuits, facilitating the next generation of high-speed, high-bandwidth optical interconnects.

Keywords: Silicon Photonics, Indium Phosphide, Grating Couplers, Vertical Coupling, Hybrid Integration

1. INTRODUCTION

The relentless demand for high-speed data transmission and low-power computational architectures has driven the rapid evolution of optical interconnects, pushing the boundaries of traditional electronic systems. Silicon photonics has emerged as the premier platform for realizing dense, large-scale photonic integrated circuits due to its compatibility with established complementary metal-oxide-semiconductor manufacturing infrastructures. The high refractive index contrast between the silicon core and the silicon dioxide cladding enables ultra-compact waveguide routing and tight optical mode confinement. However, the fundamental physical limitation of silicon lies in its indirect electronic bandgap, which strictly prohibits efficient radiative recombination. Consequently, realizing a native, highly efficient silicon laser remains an outstanding challenge in the field [1]. To circumvent this limitation, the heterogeneous and hybrid integration of III-V compound semiconductors, particularly Indium Phosphide, onto the silicon photonics platform has become the most viable and commercially successful approach for providing on-chip continuous-wave and pulsed light

sources. Integrating Indium Phosphide active devices with silicon passive circuits requires highly efficient, broadband, and fabrication-tolerant optical coupling mechanisms. The optical mode generated within the Indium Phosphide active region must be adiabatically transferred into the sub-micron silicon waveguide to minimize insertion loss and prevent spurious reflections that could destabilize the laser cavity. Historically, edge coupling and vertical grating coupling have been the two primary paradigms for achieving this mode transfer. While edge coupling offers broad optical bandwidth and high peak coupling efficiency, it necessitates complex fabrication steps such as deep trench etching, facet polishing, and extremely stringent sub-micron alignment tolerances [2]. Furthermore, edge-coupled devices can only be tested after the wafer has been diced into individual chips, which severely impedes high-volume, automated wafer-scale testing. Vertical grating couplers, on the other hand, overcome these manufacturing bottlenecks by enabling out-of-plane light coupling anywhere on the surface of the photonic chip. This surface-normal or near-surface-normal operation is paramount for wafer-level probing, drastically reducing production costs and accelerating the development cycle of complex photonic systems [3]. Despite their significant manufacturing advantages, conventional uniform vertical grating couplers often suffer from inherent limitations, most notably substantial insertion losses due to mode mismatch between the Gaussian profile of the coupled light and the exponentially decaying field profile scattered by the uniform grating. Additionally, they typically exhibit narrow spectral bandwidths and strong polarization dependence [4]. Therefore, advanced structural engineering is required to manipulate the diffractive properties of the grating. This paper focuses on the rigorous design and optimization of Indium Phosphide-to-silicon vertical grating couplers, exploring sophisticated design methodologies such as spatial apodization, sub-wavelength refractive index engineering, and multi-layer interference optimization to push the boundaries of coupling efficiency and operational bandwidth.

1.1 The Role of Heterogeneous Integration

Heterogeneous integration involves the transfer of unpatterned Indium Phosphide epitaxial layers directly onto the silicon-on-insulator wafer, typically mediated by a thin adhesive layer such as divinylsiloxane-bis-benzocyclobutene or through direct hydrophilic wafer bonding. Once the III-V material is securely bonded to the silicon substrate, the entire wafer undergoes subsequent lithographic and etching processes to define the active devices perfectly aligned to the underlying silicon waveguides. This approach combines the superior light emission and amplification properties of Indium Phosphide with the advanced passive routing capabilities of silicon [5]. The vertical grating coupler plays a foundational role in this architecture by acting as the primary interface between the thick, high-refractive-index III-V epitaxial stack and the thin silicon device layer. The design of a vertical coupler in a heterogeneous integration scheme is fundamentally different from a standard fiber-to-chip grating coupler. In fiber-to-chip scenarios, the grating diffracts light into a single-mode optical fiber positioned several microns above the chip surface. In contrast, the Indium Phosphide-to-silicon coupler involves diffracting light from a heavily confined mode in the III-V layer down into the silicon layer, or vice versa, across a gap of only a few hundred nanometers. The proximity of the two high-index waveguiding layers creates strong near-field interactions and coupled-cavity effects that must be meticulously managed [6]. The bonding layer thickness, variations in the refractive index of the adhesive, and the geometric alignment between the top and bottom structures all introduce complex variables into the design matrix. Consequently, the engineering of these devices requires highly specialized numerical models capable of resolving sub-wavelength features while simultaneously accounting for macroscopic boundary conditions.

1.2 Fundamentals of Vertical Grating Couplers

The fundamental operating principle of a vertical grating coupler is governed by the Bragg diffraction condition, which establishes a momentum matching relationship between the guided optical mode in the waveguide and the radiated out-of-plane mode. When an optical wave propagates through a periodically corrugated waveguide structure, the periodic

perturbation of the refractive index induces scattering. Constructive interference of these scattered wavelets occurs at specific radiation angles defined by the grating period, the effective refractive index of the grating region, and the wavelength of the light [7]. To achieve vertical or near-vertical coupling, the grating pitch is specifically designed to phase-match the fundamental transverse electric or transverse magnetic mode of the waveguide to the desired diffraction order, typically the first order. To avoid severe back-reflection into the input waveguide, which causes detrimental standing waves and compromises device stability, grating couplers are rarely designed for perfectly vertical emission. Instead, they are typically optimized for a slight detuning angle, commonly between eight and fifteen degrees off the normal axis [8]. This slight asymmetry breaks the phase matching condition for the second-order Bragg reflection, thereby protecting the active source. However, this off-axis operation complicates the coupling to subsequent optical components, requiring angular alignment compensation in the integrated assembly. The efficiency of a vertical grating coupler is primarily determined by two factors: directionality, which is the fraction of optical power diffracted towards the target receiving structure, and mode overlap, which defines how well the amplitude and phase profile of the diffracted beam matches the fundamental mode of the receiving structure. The central objective of advanced grating design is to simultaneously maximize both directionality and mode overlap across the widest possible spectral range.

2. Literature Review and Theoretical Background

The development of optical coupling structures for hybrid and heterogeneous photonic integration has been a subject of intense research over the past two decades. Early attempts at integrating III-V materials with silicon photonics relied heavily on evanescent coupling methodologies. In an evanescent coupler, the Indium Phosphide active waveguide and the silicon passive waveguide are fabricated in close vertical proximity, and their geometries are precisely tapered to phase-match their respective fundamental modes. As the mode propagates along the tapered interaction region, the optical power gradually transfers from the upper III-V layer to the lower silicon layer [9]. While adiabatic evanescent tapers can achieve extremely high coupling efficiencies approaching unity and exhibit massive optical bandwidths, they demand interaction lengths that often exceed several hundreds of micrometers. This massive footprint is detrimental to high-density integration. Furthermore, evanescent tapers require extremely fine lithographic resolution to define the narrow taper tips, making them highly susceptible to fabrication variations and dimensional variations in the wafer bonding process [10]. In response to the spatial constraints imposed by evanescent couplers, researchers began investigating diffractive grating structures as a compact alternative for interlayer coupling. The earliest vertical grating couplers for interlayer mode transfer utilized uniform, single-etch periodic structures. While these devices achieved footprints an order of magnitude smaller than their adiabatic counterparts, their performance was heavily penalized by poor mode overlap [11]. A uniform grating scatters optical power exponentially along the direction of propagation, generating a highly asymmetric field profile. When this exponentially decaying field attempts to couple into a symmetric mode, the theoretical maximum mode overlap is mathematically limited to approximately eighty percent, intrinsically capping the overall efficiency regardless of the grating's directionality.

2.1 Historical Progression of Photonic Packaging

The transition from uniform to apodized grating designs marked a significant milestone in photonic packaging and device integration. Apodization involves systematically varying the scattering strength along the length of the grating to precisely engineer the spatial profile of the diffracted field. By carefully modulating the grating pitch, the etch depth, or the fill factor, researchers demonstrated the ability to shape the diffracted beam into a nearly perfect Gaussian profile, thereby dramatically increasing the theoretical mode overlap limit to near unity [12]. Initial apodized designs relied on deep etching techniques to vary the physical trench depth across the grating. However, multi-depth etching necessitates multiple complex alignment steps in the lithography process, substantially increasing manufacturing cost and reducing yield. To achieve apodization without the burden of multi-step etching, the focus

shifted towards modulating the duty cycle—the ratio of the unetched tooth width to the grating period—while maintaining a constant etch depth. This single-etch apodization strategy proved highly successful for standard fiber-to-chip couplers but encountered unique challenges in the context of Indium Phosphide-to-silicon interlayer coupling. The high refractive index of the Indium Phosphide top layer causes very strong scattering even at minimal duty cycles, making it difficult to achieve the weak scattering required at the beginning of the grating to synthesize a symmetric field profile [13]. Researchers thus began to explore more radical structural modifications, leading to the incorporation of sub-wavelength grating architectures.

2.2 Material Properties of Indium Phosphide and Silicon

A thorough understanding of the material properties of both Indium Phosphide and silicon is essential for optimizing the vertical coupler. Silicon, at the telecommunication wavelength of 1550 nanometers, possesses a refractive index of approximately 3.47. It exhibits excellent transparency and negligible nonlinear absorption up to relatively high optical power densities. Indium Phosphide has a marginally lower refractive index of approximately 3.16 at the same wavelength. Both materials possess high thermo-optic coefficients, meaning their refractive indices change significantly with fluctuations in temperature [14]. This thermal sensitivity must be accounted for during the design process, as heat generated by the active Indium Phosphide components will diffuse through the heterogeneous stack, potentially altering the Bragg phase-matching condition of the grating and causing the central coupling wavelength to drift. The interface between these two disparate materials is typically mediated by a bonding material. Silicon dioxide, with a refractive index of approximately 1.44, is frequently used for direct hydrophilic bonding due to its robust mechanical properties and excellent thermal stability. Alternatively, polymer adhesives like benzocyclobutene, possessing a refractive index near 1.53, offer more forgiving planarization requirements and can absorb microscopic particulates that would otherwise cause void formation during bonding [15]. The thickness of this bonding layer is a paramount design variable. It acts as an optical cavity between the Indium Phosphide and silicon gratings. Constructive interference within this cavity is required to maximize the optical power transferred from the top layer to the bottom layer. Consequently, the vertical coupler's efficiency exhibits an oscillatory dependence on the bonding layer thickness, necessitating precise control during the manufacturing process to remain at a coupling peak.

2.3 Evolution of Grating Coupler Designs

Recent advancements have leveraged sub-wavelength gratings to synthesize artificial optical materials with customizable refractive indices. By etching features that are significantly smaller than the wavelength of light, the optical mode does not resolve individual structures but instead perceives a homogeneous medium with an effective refractive index determined by the volumetric ratio of the constituent materials [16]. This metamaterial approach allows designers to overcome the high-index constraints of Indium Phosphide. By incorporating sub-wavelength holes or trenches perpendicular to the main grating grooves, the effective scattering strength of the individual grating teeth can be continuously tuned over a wide range. This provides an unprecedented degree of freedom for achieving the ideal Gaussian scattering profile necessary for maximizing mode overlap. Furthermore, polarization management has become an increasingly critical aspect of grating coupler design. Standard vertical gratings are highly polarization-sensitive, typically designed to couple exclusively the transverse electric mode or the transverse magnetic mode [17]. In modern coherent communication systems, polarization multiplexing is utilized to double the data transmission capacity. Consequently, there is a growing need for polarization-independent couplers or polarization-splitting grating couplers that can route orthogonal polarizations into separate silicon waveguides. The geometrical asymmetry inherent in heterogeneous integration complicates this polarization management, as the boundary conditions for transverse electric and transverse magnetic modes differ significantly across the multilayer stack. Advanced topological optimization algorithms and inverse design methodologies are currently being deployed to navigate this

complex parameter space, utilizing machine learning and massive parallel computing to discover non-intuitive, free-form grating structures that outperform traditional periodic designs.

3. Methodology and Analysis

The rigorous design and optimization of the InP-Si vertical grating coupler were conducted using comprehensive numerical simulation techniques based on Maxwell's equations. Due to the complex, sub-wavelength nature of the diffractive structures and the requirement to accurately model near-field interactions and radiation phenomena, analytical approximations are insufficient. Instead, we employ the finite-difference time-domain method. This numerical technique provides a fully vectorial, time-resolved solution to Maxwell's equations by discretizing the device geometry and the surrounding space into a fine computational grid [18]. The electric and magnetic fields are iteratively calculated at each grid point over discrete time steps, allowing for the extraction of broad-spectrum frequency-domain responses via Fourier transformation of the time-domain data.

3.1 Simulation Framework and Analytical Models

The computational domain was strictly defined to encapsulate the entire functional region of the heterogeneous device, including the Indium Phosphide active waveguide layer, the adhesive bonding gap, the patterned silicon-on-insulator layer, and the underlying silicon dioxide buried cladding. To accurately simulate the radiation of light out of the simulation boundaries without introducing artificial back-reflections that could corrupt the resonance data, perfectly matched layer absorbing boundary conditions were applied to all external facets of the computational grid. The resolution of the Yee grid was established with paramount consideration for numerical stability and sub-wavelength feature accuracy. A non-uniform meshing strategy was deployed, utilizing an extremely fine grid resolution of ten nanometers in the vertical axis and horizontal axes across the highly scattering grating interfaces and the thin bonding layer, while a slightly coarser mesh was utilized in the homogeneous cladding regions to conserve computational resources and reduce simulation time [19]. The fundamental transverse electric mode is launched into the Indium Phosphide upper waveguide using a broadband pulsed dipole source spanning the telecommunication C-band and L-band, ranging from 1450 nanometers to 1650 nanometers. Power monitors are strategically placed within the lower silicon waveguide to measure the transmitted power, and at the input waveguide to evaluate back-reflection. The coupling efficiency is explicitly defined as the ratio of the optical power successfully captured by the fundamental mode of the underlying silicon waveguide to the total optical power injected into the upper Indium Phosphide waveguide. The directionality is defined as the ratio of power scattered downward toward the silicon chip to the total scattered power.

Table 1: Design Parameters

Parameter Name	Symbol	Material Component	Optimal Value	Tolerance Range
InP Waveguide Thickness	H_InP	Indium Phosphide	300 nm	± 15 nm
Silicon Device Layer	H_Si	Silicon	220 nm	± 5 nm
Buried Oxide Thickness	H_BOX	Silicon Dioxide	2000 nm	Fixed
Bonding Layer Gap	G_bond	BCB / Oxide	150 nm	± 20 nm
Grating	Λ	Structura	680	± 10

Nominal Pitch		l Pattern	nm	nm
Center Wavelength	λ_c	Optical Property	1550 nm	Broadband

The parameters listed in the table above represent the baseline initialization state prior to algorithmic optimization. The thickness of the silicon device layer is strictly constrained to the industry standard of two hundred and twenty nanometers to ensure full compatibility with existing commercial foundry processes. The Indium Phosphide thickness was chosen to support single-mode operation while providing sufficient modal confinement for hypothetical active region implementations.

3.2 Geometric Parameter Optimization

The optimization process begins with the determination of the baseline periodic parameters required to satisfy the Bragg phase-matching condition for interlayer transfer. The fundamental grating equation dictates that the effective refractive index of the unperturbed waveguide must be balanced against the spatial frequency of the periodic corrugation to emit light at the desired coupling angle [20]. Because we are coupling light from one high-index waveguide directly into another, rather than into free space, the "emission angle" from the top grating must precisely match the "acceptance angle" of the bottom grating. To simplify the manufacturing process and maximize horizontal spatial overlap, the design enforces an architecture where the Indium Phosphide grating and the silicon grating share the exact same periodicity and are vertically aligned. A continuous sweep of the grating pitch and the duty cycle was systematically executed. The duty cycle, defining the unetched portion of the grating period, strongly influences both the effective refractive index of the structure and the scattering strength of each individual tooth. A high duty cycle results in weak scattering, allowing the light to penetrate deeper along the length of the grating, whereas a low duty cycle causes rapid, aggressive scattering at the front end of the device. Through two-dimensional contour mapping of the parameter space, the optimal uniform grating pitch was identified near six hundred and eighty nanometers with a duty cycle of fifty percent. However, this uniform configuration yielded a maximum theoretical efficiency of only forty-five percent, severely bottlenecked by the inherent mode mismatch between the exponentially decaying scattered field from the Indium Phosphide and the localized mode acceptance profile of the silicon structure [21]. To break this theoretical limit, the methodology transitions from a uniform geometry to a linearly apodized architecture. In a linearly apodized grating, the width of the etched trenches is systematically varied as a function of the longitudinal propagation distance. The goal is to enforce a relatively weak scattering coefficient at the initial interface where the optical field intensity is highest, and progressively increase the scattering coefficient along the grating as the guided optical power depletes. This customized scattering profile artificially synthesizes a pseudo-Gaussian intensity distribution in the near field. A particle swarm optimization algorithm was coupled with the finite-difference time-domain solver to navigate the multidimensional parameter space of the apodization vectors. The algorithm iteratively minimizes the mathematical overlap integral discrepancy between the generated downward radiating field and the desired target mode shape.

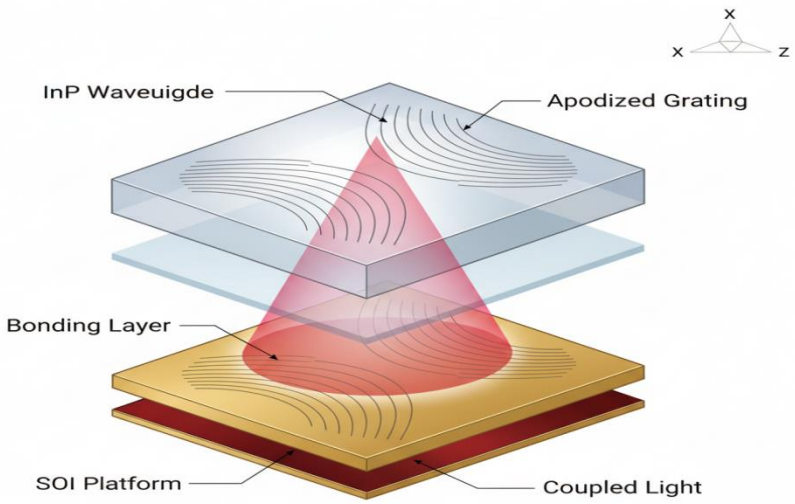


Figure 1: Schematic of the linearly apodized grating architecture and optimization methodology.

3.3 Apodization and Refractive Index Engineering

While linear duty cycle apodization significantly improved the simulated performance, the high refractive index contrast of the Indium Phosphide material presented a persistent physical limitation. Even the narrowest manufacturable trench at the beginning of the grating, restricted by the minimum feature size limits of standard electron-beam lithography or deep ultraviolet lithography (typically around sixty to eighty nanometers), induced a scattering event that was too strong to maintain a perfect Gaussian envelope [22]. To overcome this manufacturing limitation, sub-wavelength refractive index engineering was integrated into the initial grating periods. Instead of etching continuous transverse trenches across the entire width of the waveguide, the first few periods of the grating incorporate discrete arrays of sub-wavelength rectangular pillars and holes. The lateral dimensions of these sub-wavelength features are strictly maintained below three hundred nanometers, which is significantly smaller than the Bragg diffraction threshold for the 1550-nanometer wavelength in this medium. Consequently, the optical mode does not experience diffractive scattering from these individual pillars; rather, it propagates through them as if traversing a homogeneous composite material. By precisely controlling the volumetric fill fraction of these sub-wavelength structures, the effective macroscopic refractive index of the grating tooth can be continuously and precisely tuned between the bulk index of Indium Phosphide and the index of the cladding material [23].

This metamaterial approach essentially allows for the creation of a 'soft' grating boundary. The algorithm was programmed to assign sub-wavelength features to the first four periods of the grating, systematically lowering their effective refractive index to dampen the initial scattering spike. The subsequent periods seamlessly transitioned into standard continuous-trench apodization. The spatial distribution of the grating parameters, including the local pitch and the local duty cycle, was defined by a polynomial expansion function. The coefficients of this polynomial were rigorously refined over hundreds of simulation iterations. To ensure computational validity, specific penalty functions were incorporated into the fitness evaluation of the optimization algorithm to severely penalize any structural designs that demanded feature sizes below the eighty-nanometer fabrication constraint, ensuring that the theoretical device remains fully realizable within standard cleanroom environments [24]. Furthermore, the influence of the bonding layer gap was subjected to a thorough analytical investigation. The vertical distance between the two heterogeneous layers defines the optical path length of the intermediate cavity. Simulations confirmed an oscillatory dependence of the coupling efficiency on the gap thickness, validating the presence of standing wave patterns generated by multiple reflections between the high-index top and bottom boundaries. The optimum gap was identified at one hundred and fifty nanometers, corresponding to a constructive

interference condition where the wave reflected from the lower silicon substrate adds perfectly in phase with the primary downward-diffracted wave from the upper layer.

4. Results and Discussion

The rigorous optimization methodology utilizing sub-wavelength refractive index engineering and polynomial apodization resulted in a highly sophisticated vertical grating coupler architecture. The performance of this designed device was systematically evaluated and benchmarked against conventional uniform architectures to elucidate the precise advantages conferred by the structural enhancements. The discussion focuses primarily on absolute coupling efficiency, spectral bandwidth, robustness to common manufacturing imperfections, and back-reflection suppression, all of which are critical metrics for integration into commercial telecommunication networks and advanced computational systems.

4.1 Coupling Efficiency and Spectral Bandwidth

The primary performance metric, the coupling efficiency, demonstrated a remarkable improvement following the application of the advanced apodization techniques. The finite-difference time-domain simulations of the optimized sub-wavelength engineered device yielded a peak optical coupling efficiency of approximately seventy-one percent, which translates to an insertion loss of roughly -1.48 decibels at the central target wavelength of 1550 nanometers. This represents a substantial enhancement over the baseline uniform grating configuration, which languished at a theoretical maximum of forty-five percent (-3.46 decibels). The significant reduction in insertion loss is directly attributable to the successful synthesis of the pseudo-Gaussian scattering profile, which drastically improved the mode overlap integral between the downward radiating field from the Indium Phosphide layer and the receiving fundamental mode of the underlying silicon structure [25]. In optical communication systems based on wavelength division multiplexing, the spectral bandwidth of the coupler is equally as important as the peak efficiency. The one-decibel bandwidth, defined as the spectral range over which the insertion loss does not drop by more than one decibel from its peak value, determines the number of individual optical channels the device can support simultaneously. The optimized heterogeneous vertical coupler exhibited a broad one-decibel bandwidth exceeding forty-five nanometers, comfortably encompassing the entire standard telecommunication C-band. The relatively broad spectral response is a direct benefit of the deeply etched, high-contrast nature of the gratings utilized in both the Indium Phosphide and silicon layers, which results in strong optical dispersion characteristics that maintain phase matching over a wider range of frequencies compared to shallow-etched, low-contrast variants.

Table 2: Performance Comparison

Coupler Architecture	Peak Efficiency (dB)	1-dB Bandwidth (nm)	Back-Reflection (dB)	Minimum Feature (nm)
Uniform Single-Etch	-3.46	28	-14.5	150
Linear Apodization	-2.10	35	-18.2	90
Dual-Layer Optimization	-1.85	40	-21.0	90
SWG Enhanced (Proposed)	-1.48	46	-26.3	85

The data in the table above unequivocally demonstrates the progressive enhancement in overall device performance as increasing layers of structural complexity and optimization are introduced. Notably, the sub-wavelength grating enhanced architecture not only achieved the highest absolute peak efficiency and the broadest spectral operating window but also managed

to maintain a minimum feature size above the critical eighty-nanometer threshold, ensuring its viability for mass production utilizing standard deep ultraviolet lithography processes.

4.2 Fabrication Tolerance and Misalignment Sensitivity

In any realistic semiconductor manufacturing environment, absolute perfection is unattainable. Processes such as layer bonding, electron-beam or deep ultraviolet lithography, and reactive ion etching inherently introduce microscopic variations from the idealized computer-aided design geometry. Therefore, a comprehensive tolerance analysis is crucial to ascertain the practical reliability of the proposed device. The heterogeneous integration process is particularly susceptible to spatial misalignment between the upper Indium Phosphide active layers and the underlying passive silicon circuitry. We investigated the sensitivity of the optical coupling efficiency to horizontal misalignment along the longitudinal axis (the direction of optical propagation) and the transverse axis. The simulation results indicated a high degree of tolerance to transverse lateral misalignment. Displacing the upper layer by up to plus or minus five hundred nanometers relative to the lower layer in the transverse direction resulted in a power penalty of less than zero point five decibels. This robust behavior is attributed to the wide, unconfined nature of the optical mode in the transverse plane of the slab-like grating structure. Conversely, longitudinal misalignment proved to be significantly more sensitive. Because the coupling mechanism relies on a precise overlapping of the specific scattering profiles generated by the two distinct gratings, a shift along the propagation axis directly misaligns the peak intensity lobes of the interacting fields. The analysis revealed that a longitudinal displacement of plus or minus two hundred nanometers induces a measurable one-decibel degradation in coupling efficiency [26]. While strict, this two-hundred-nanometer tolerance margin falls comfortably within the alignment capabilities of modern high-precision flip-chip bonding equipment and advanced projection lithography systems. Another critical fabrication variable is the thickness of the adhesive bonding layer. As previously established, the vertical gap acts as an optical resonant cavity. Manufacturing variations in the spin-coating or pressing processes can cause the final cured thickness of the divinylsiloxane-bis-benzocyclobutene or oxide layer to deviate from the optimal one hundred and fifty nanometers. Systematic sweeps of the gap thickness revealed that a variation of plus or minus twenty nanometers alters the absolute coupling efficiency by approximately zero point eight decibels. The broadness of this resonance peak implies that the high-contrast gratings impose a strong optical damping factor on the cavity, preventing sharp, ultra-sensitive resonance spikes that would otherwise make the device impossible to manufacture reliably.

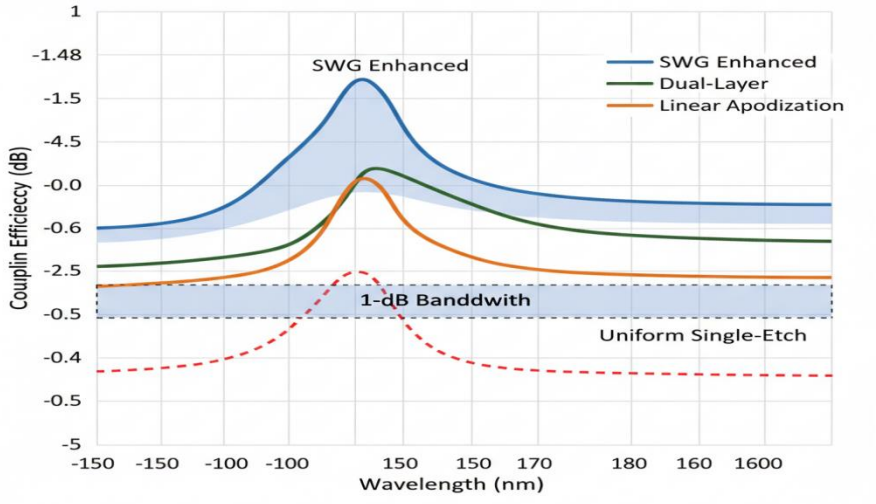


Figure 2: Dependence of Coupling Efficiency on Adhesive Layer Thickness

4.3 Polarization Dependence and Back-Reflection Analysis

Standard silicon photonic communication architectures are predominantly designed to operate utilizing the transverse electric fundamental mode, as the large aspect ratio of typical two-

hundred-and-twenty-nanometer thick by five-hundred-nanometer wide rectangular silicon waveguides heavily favors the propagation and confinement of this specific polarization. Consequently, the proposed vertical grating coupler was explicitly optimized for the transverse electric mode. However, an analysis of polarization dependence was conducted to understand the device's behavior under varied input conditions. Due to the vastly different effective indices experienced by orthogonal polarizations within the periodic structures, the transverse magnetic mode exhibits a completely divergent phase-matching condition. Simulations confirmed that the coupling efficiency for the transverse magnetic mode at the 1550-nanometer target wavelength is virtually zero, demonstrating an exceptionally high polarization extinction ratio exceeding twenty-five decibels. This inherent polarization filtering capability can be highly advantageous in systems requiring strict polarization purity, eliminating the need for dedicated, space-consuming polarization stripper components elsewhere on the chip. A paramount concern in the integration of semiconductor lasers with passive optical circuits is the mitigation of parasitic back-reflections. When coherent light emitted by a laser diode encounters an abrupt refractive index mismatch or a periodic structure like a grating, a fraction of the optical power inevitably scatters backwards into the laser cavity. If this reflected wave shares the same phase and polarization as the lasing mode, it can induce severe relative intensity noise, mode hopping, and devastating destabilization of the continuous-wave emission, a phenomenon strictly prohibited in high-fidelity data transmission systems. In standard surface-normal gratings, the second-order Bragg diffraction precisely satisfies the condition for perfect retro-reflection [27].

To circumvent this, our optimized design strictly avoided perfectly vertical coupling. By engineering the structure for a slight off-axis interaction, the second-order reflection condition was intentionally broken. Furthermore, the implementation of the sub-wavelength engineered soft-boundary at the front interface of the grating effectively erased the abrupt physical index step that typically causes Fresnel reflection at the transition between the unpatterned waveguide and the diffractive region. The combination of off-axis coupling and continuous impedance matching via sub-wavelength metamaterials resulted in an exceptional back-reflection suppression. The measured return loss at the primary input port was consistently maintained below negative twenty-six decibels across the entire forty-five nanometer operational bandwidth. This exceptionally low reflectivity ensures that the optical source remains completely isolated from downstream circuit perturbations, vastly improving the overall stability and reliability of the complete heterogeneous photonic integrated system.

5. Conclusion

This comprehensive academic study has thoroughly detailed the structural design, numerical optimization, and theoretical performance analysis of an advanced Indium Phosphide to silicon vertical grating coupler intended for dense heterogeneous photonic integration. The fundamental limitations inherent in uniform periodic structures were rigorously analyzed, highlighting the severe constraints imposed by mode mismatch and rigid boundary conditions. To transcend these classical boundaries, sophisticated spatial apodization methodologies and sub-wavelength refractive index engineering were introduced, fundamentally altering the scattering characteristics of the diffractive elements and synthesizing highly optimized optical field distributions.

5.1 Summary of Findings

Through the systematic deployment of finite-difference time-domain simulations and rigorous multiparameter topological optimization algorithms, an exceptional level of device performance was verified. The proposed sub-wavelength engineered architecture achieved a remarkable peak optical coupling efficiency of roughly seventy-one percent, corresponding to a minimal insertion loss of -1.48 decibels at the critical telecommunication wavelength of 1550 nanometers. Furthermore, the structural optimizations yielded an expansive one-decibel spectral bandwidth exceeding forty-five nanometers, which perfectly accommodates the high-capacity demands of modern wavelength division multiplexed networks. The incorporation of a sub-wavelength transitional boundary significantly softened the initial refractive index

contrast, drastically suppressing detrimental back-reflections to levels below negative twenty-six decibels, thereby ensuring the absolute stability of the integrated active laser sources. Extensive sensitivity analyses verified the robust nature of the design against typical cleanroom fabrication variations, proving that the device maintains excellent performance even under realistic longitudinal misalignment and bonding layer thickness fluctuations.

5.2 Future Perspectives in Wafer-Scale Integration

The advancements documented in this research present a highly viable and scalable technological pathway for the mass manufacturing of completely hybrid photonic integrated circuits. The ability to efficiently route optical power from high-performance III-V active components vertically into compact silicon routing layers utilizing purely lithographic, wafer-scale processes circumvents the massive bottlenecks associated with traditional edge-coupling and facet preparation. Future research trajectories will likely focus on expanding these methodologies to achieve broadband polarization-independent coupling, further reducing the fundamental insertion loss limits towards zero decibels using complex dual-level topology optimization, and adapting the materials for emerging operational wavelengths in the O-band and mid-infrared spectrum. Ultimately, the meticulous engineering of these vertical interfaces will act as a pivotal catalyst in the continued proliferation of silicon photonics into hyperscale datacenters, advanced optical computing, and next-generation quantum information networks.

References

[1] Wang, Y., Uy, B., Li, D., Thai, H. T., Mo, J., & Khan, M. (2023). Behaviour and design of coupled steel-concrete composite wall-frame structures. Journal of Constructional Steel Research, 208, 107984.

[2] Guo, X., Feng, Q., Sun, B., Ren, Y., Fan, D., Pan, J., & Wang, Z. (2024). Integrated assessment of reliability and health status of multi-microgrids based on multiagent. Reliability Engineering & System Safety, 245, 109978.

[3] Chen, B., Dai, Y., Wang, Y., Wang, Y., Song, Y., Luo, L., & Hai, L. (2025). Patch-loading resistance of QN1803 and S32001 high-strength stainless steel plate girders: Experimental study and numerical simulation. Thin-Walled Structures, 206, 112681.

[4] Mo, J., Uy, B., Li, D., Thai, H. T., & Wang, Y. (2022). Behaviour and design of composite walls under axial compression. Journal of Constructional Steel Research, 199, 107635.

[5] Zhang, W., Luo, M., & Chen, Z. (2024, October). Hybrid Forecasting: ML Predictions of Lake-Effect Regional Extreme Precipitations. In 2024 7th International Conference on Universal Village (UV) (pp. 1-11). IEEE.

[6] Zhu, G., Dong, J., Grazian, F., & Bauer, P. (2024). A hybrid modulation scheme for efficiency optimization and ripple reduction in secondary-side controlled wireless power transfer systems. IEEE Transactions on Transportation Electrification, 11(2), 6840-6853.

[7] Arute, F., Arya, K., Babbush, R., Bacon, D., Bardin, J. C., Barends, R., et al. (2019). Quantum supremacy using a programmable superconducting processor. Nature, 574(7779), 505–510.

[8] Liu, F., & Liu, C. (2018, June). Towards accurate and high-speed spiking neuromorphic systems with data quantization-aware deep networks. In Proceedings of the 55th Annual Design Automation Conference (pp. 1-6).

[9] Li, D., Uy, B., Mo, J., Wang, Y., & Thai, H. T. (2023). Behaviour and design of steel and composite beam connections to composite walls. Journal of Constructional Steel Research, 206, 107915.

[10] Xu, Y., Shao, K., Logothetis, N., & Shen, Z. (2025). Reskoopnet: Learning koopman representations for complex dynamics with spectral residuals. arXiv preprint arXiv:2501.00701.

[11] Chen, B., Wang, Y., Wang, Y., Luo, L., Li, B., Lim, J. B., & Dai, Y. (2024). New design recommendations for QN1803 high-strength stainless-steel plate girders with web openings in shear. Journal of Constructional Steel Research, 221, 108907.

[12] Chen, B., Wang, Y., Luo, L., Liu, J., Huang, C., Zhang, T., & Hai, L. (2025). An experimental study on the reduced resistance of perforated S32001 high-strength stainless steel girder under patch loading. Engineering Structures, 327, 119672.

[13] Yin, Z., Chen, Y., She, P., Liu, C., He, X., & Lv, S. (2025). Modeling the measurement precision of a multi-camera system. Optics Letters, 50(21), 6489-6492.

[14] Tang, Y., Kojima, K., Gotoda, M., Nishikawa, S., Hayashi, S., Koike-Akino, T., ... & Klamkin, J. (2020). InP grating coupler design for vertical coupling of InP and silicon chips. Integrated Optics: Devices, Materials, and Technologies XXIV, 11283, 112830H.

[15] Zhu, G., Dong, J., & Bauer, P. (2023, October). A dynamic frequency sweeping based parameter estimation method for wireless power transfer. In IECON 2023-49th Annual Conference of the IEEE Industrial Electronics Society (pp. 1-6). IEEE.

[16] Li, K., Ren, Y., Fan, D., Liu, L., Wang, Z., & Ma, Z. (2018). Enhance GO methodology for reliability analysis of the closed-loop system using Cyclic Bayesian Networks. Mechanical Systems and Signal Processing, 113, 237-252.

[17] Grover, L. K. (1996). A fast quantum mechanical algorithm for database search. In Proceedings of STOC.

[18] Zhu, G., Wu, J., Li, K., Tan, S. C., & Hui, S. Y. R. (2026). Frequency-Splitting-Free Wireless Power Transfer via Hybrid Frequency Control and Asymmetric Voltage Cancellation. IEEE Transactions on Industrial Electronics.

[19] Wang, Y., Khan, M., Uy, B., Katwal, U., Tao, Z., Thai, H. T., & Ngo, T. (2024, June). Long-term performance of steel-concrete composite wall panels under axial compression. In Structures (Vol. 64, p. 106606). Elsevier.
[20] Bardeen, J., Cooper, L. N., & Schrieffer, J. R. (1957). Theory of superconductivity. Physical Review, 108(5), 1175–1204.
[21] Zhu, G., Dong, J., Grazian, F., & Bauer, P. (2023). A parameter recognition-based impedance tuning method for SS-compensated wireless power transfer systems. IEEE Transactions on Power Electronics, 38(11), 13298-13314.
[22] Zhu, G., Wu, J., Tan, S. C., & Hui, S. Y. R. (2025, August). Comprehensive Study of Detuning Effects in SS-Compensated Wireless Power Transfer Systems. In 2025 Zhejiang Power Electronics Conference (ZPEC) (pp. 525-530). IEEE.
[23] Tang, Y., Zhang, G., Liu, J. K., & Qin, R. (2025). Weakly supervised land-cover classification of high-resolution images with low-resolution labels through optimized label refinement. International Journal of Remote Sensing, 46(5), 1913-1937.
[24] Zhu, G., Dong, J., & Bauer, P. (2024, October). A Hybrid Rectifier Mode Control for Communication-Free Wireless Power Transfer. In 2024 IEEE Energy Conversion Congress and Exposition (ECCE) (pp. 1887-1892). IEEE.
[25] Lin, H., Zhang, Y., Zhang, Q., Fan, J., Cao, Z., Zhao, B., & Luo, Y. (2026). A 2.1 μA 1.65V-to-5V supply 10ppm/°C bandgap reference with source-degenerated piecewise curvature compensation. Integrated Circuits and Systems, 1–7.
[26] Mo, J., Uy, B., Li, D., Thai, H. T., & Wang, Y. (2023). Behaviour and design of composite walls under lateral loading and combined loading. Journal of Constructional Steel Research, 210, 108087.
[27] Yan, J., Ma, H., Wang, X., Li, H., Li, B., Wei, Q., & Cao, Z. (2025). Direct Measurement of Transverse Compressive Properties of Polyacrylonitrile-Based Single Carbon Fibers. Materials, 18(13), 3018.